SANDIA REPORT
SAND2015-7964
UNCLASSIFIED
Printed September 2015

Precision Laser Annealing of Focal Plane Arrays

Daniel A. Bender, Christopher T. DeRose, Andrew Starbuck, Jason C. Verley and Mark W. Jenkins

Prepared by
Sandia National Laboratories
Albuquerque, New Mexico 87185 and Livermore, California 94550

Sandia National Laboratories is a multi-program laboratory managed and operated by Sandia Corporation, a wholly owned subsidiary of Lockheed Martin Corporation, for the U.S. Department of Energy's National Nuclear Security Administration under contract DE-AC04-94AL85000.

Issued by Sandia National Laboratories, operated for the United States Department of Energy by Sandia Corporation.

Available to DOE and DOE contractors from
U.S. Department of Energy
Office of Scientific and Technical Information
P.O. Box 62
Oak Ridge, TN 37831

Telephone: (865) 576-8401
Facsimile: (865) 576-5728
E-Mail: reports@adonis.osti.gov
Online ordering: http://www.osti.gov/bridge

Available to the public from
U.S. Department of Commerce
National Technical Information Service
5285 Port Royal Rd.
Springfield, VA 22161

Telephone: (800) 553-6847
Facsimile: (703) 605-6900
E-Mail: orders@ntis.fedworld.gov
Online order: http://www.ntis.gov/help/ordermethods.asp?loc=7-4-0#online

SAND2015-7964

Printed September 2015

Precision Laser Annealing of Focal Plane Arrays

Daniel A. Bender
Intelligent Sensing Systems

Christopher DeRose
Applied Photonic Microsystems

Andrew Starbuck
Rad Hard CMOS Technology

Jason C. Verley
Electrical Models & Simulation

Mark W. Jenkins
Validation & Failure Analysis

Sandia National Laboratories
P.O. Box 5800
Albuquerque, NM 87185-1179

ABSTRACT

We present results from laser annealing experiments in Si using a passively Q-switched Nd:YAG microlaser. Exposure with laser at fluence values above the damage threshold of commercially available photodiodes results in electrical damage (as measured by an increase in photodiode dark current). We show that increasing the laser fluence to values in excess of the damage threshold can result in annealing of a damage site and a reduction in detector dark current by as much as 100x in some cases. A still further increase in fluence results in irreparable damage. Thus we demonstrate the presence of a laser annealing window over which performance of damaged detectors can be at least partially reconstituted. Moreover dark current reduction is observed over the entire operating range of the diode indicating that device performance has been improved for all values of reverse bias voltage. Additionally, we will present results of laser annealing in Si waveguides. By exposing a small (<10 um) length of a Si waveguide to an annealing laser pulse, the longitudinal phase of light acquired in propagating through the waveguide can be modified with high precision, <15 milliradian per laser pulse. Phase tuning by 180 degrees is exhibited with multiple exposures to one arm of a Mach-Zehnder interferometer at fluence values below the morphological damage threshold of an etched Si waveguide. No reduction in optical transmission at 1550 nm was found after 220 annealing laser shots. Modeling results for laser annealing in Si are also presented.

Contents

SAND2015-7964

Printed September, 2015

LIST OF FIGURES

This Page Intentionally Left Blank

1. INTRODUCTION

Implementation of techniques to reduce dark current and noise on detectors offers potential deep impact to the quality of data gathered and processed by optical sensors and in particular focal plane arrays (FPAs). Ideally, such techniques would precisely target only pixels or clusters of pixels that are "hot" or noisy while leaving functional pixels untouched. Laser annealing provides a means to target problematic pixels delivering a localized amount of heat allowing them to reform under the conditions of a thermal anneal without affecting surrounding detector areas or readout circuitry.

Detectors of optical signals often undergo thermal annealing in manufacturing to allow dopant activation, thermal oxidation, metal reflow and chemical vapor deposition. Thermal annealing is typically done with equipment that heats the entire semiconductor wafer by using a lamp, hot plate or furnace. Lasers are also employed typically with a cylindrical lens focusing a beam into a line that is swept across the wafer, homogenizing the surface. The research described in this paper demonstrates laser annealing as an augmentation to thermal annealing on detectors after they have been hybridized with readout electronics and packaged or as a means of reconstituting lost detector capability from damaging laser exposure. For FPAs it is only after hybridization that problematic pixels or pixel clusters emerge. Once defective regions have been identified, tailored laser irradiance can be deployed to heat pixels locally. The localization means high anneal temperatures beyond what an entire focal plane assembly can withstand are reached and will be entirely localized to the vicinity of the defect. Because laser beams can be focused to spot sizes much smaller than a pixel, single pixel thermal annealing is possible and allows targeting of only those pixels which exhibit unacceptable levels of noise. This "do no harm" approach ensures functional, acceptable pixels are not degraded or affected by the presence of neighboring defects while annealing.

Most pulsed laser based annealing schemes are not aimed at reducing noise, rather they are integral to the manufacturing process, for example to achieve high temperature dopant activation, minimizing diffusion so dopants stay where the ion implanter places them. While much research has been conducted on how to manufacture and process semiconductor materials with a laser, comparatively little thought has been given to improving device noise characteristics after an FPA has been packaged with readout electronics and before end use.

In FPAs sensor layer defects are not normally detectable until after the sensor layer is hybridized to the readout integrated circuit and tested. At this point the sensor layer cannot be taken off the readout electronics and the entire packaged assembly cannot be heated to temperatures hot enough to promote annealing. Fortunately, the location of problematic pixels or pixel clusters can be identified from characterization and testing and a tightly focused laser can be used to perform a targeted anneal. This approach is

innovative from a manufacturing perspective in that it only affects pixels with excessive noise levels and does not operate over the entire array.

Targeted laser annealing to damaged sensors or packaged FPAs prior to use represents an augmentation to state-of-the-art thermal annealing and laser procedures currently done in the manufacturing process. However, laser annealing can be done at any point after manufacturing and before use. For example, if an FPA resides in storage for several months after manufacturing, laser annealing can be used to anneal individual pixels or pixel clusters that may have degraded with time or exposure to radiation.

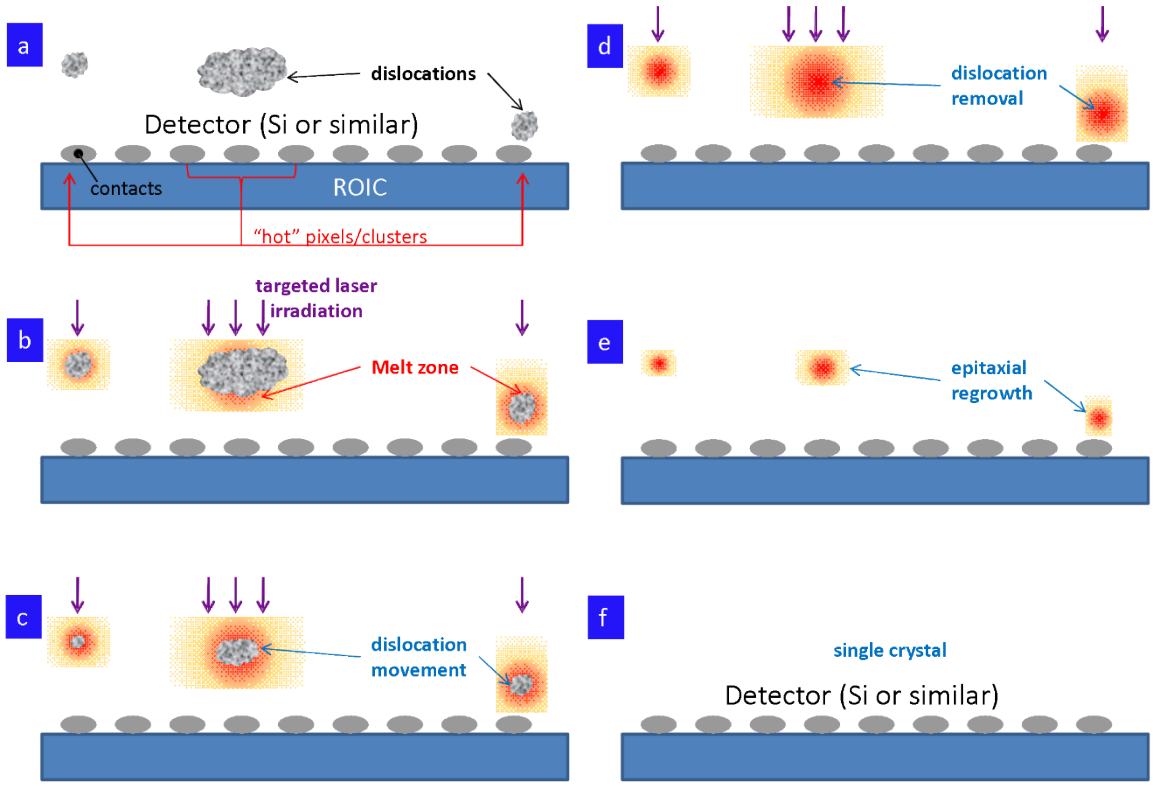

Figure 1. (a) Cross-sectional view of FPA detector and ROIC. Dislocations in the absorbing detector layer lead to increased pixel dark current and "hot" pixels in image acquisition. (b) Targeted laser irradiation heats detector material locally in the vicinity of dislocations. (c) Melted material promotes dislocation movement and lattice relaxation. (d) Dislocation removal occurs after sufficient heat deposit. (e) Surrounding unmelted regions serve as seed layers to epitaxially regrow melted zones. (f) Homogenous single crystal results after anneal.

The process of laser annealing a damaged or defective sensor is outlined in figure 1. Figure 1(a) depicts a cross-sectional view of a detector material bonded to a readout IC (ROIC); electrical contact bumps are shown. Dislocations are illustrated in the detector optical absorption region and appear over both isolated pixels and pixel cluster readouts. Interrogating the ROIC under a dark condition will reveal the location of absorbing layer dislocations due to the presence of increased pixel dark counts. With the coordinates registered for all noisy pixels, targeted laser irradiation can be directed to only those pixels with dislocations or defects, figure 1(b). The laser irradiation is intense enough to locally warm or melt the detector material. A melt zone develops around the location of the defect, allowing the material to become soft, promoting dislocation movement and

lattice relaxation, figure 1(c). Following a sufficient heat deposition (typically applied in nanoseconds) dislocations will be removed leaving only a locally melted zone, figure 1(d). After pulsed laser irradiation has concluded, regrowth of the melted zone occurs, figure 1(e). The regrowth process is epitaxial because unmelted material regions surrounding the melt zone serve as a seed layer on which the regrowth process is based. The result is a homogeneous single crystal structure, free of dislocations and defects, figure 1(f). Overall detector array performance is improved because processing is confined to dysfunctional pixels only. The annealing process here is similar to that outlined by J. Yan *et. al.* [1], but is unique in that the annealing takes place in the photodiode junction improving electrical performance, rather than on the surface repairing mechanical damage.

2. EXPERIMENTAL RESULTS

A block diagram of our experimental apparatus is shown in figure 2. The annealing laser is a diode pumped passively Q-switched Nd:YAG operating at 1064 nm and producing an 11 ns (FWHM) pulse. Maximum pulse energy is approximately 200 µJ. Output from the laser is routed through a λ/2 plate and a polarizing beamsplitter (PBS) cube to control the pulse energy. A small percentage of the laser power reflecting off the PBS is detected with a photodiode and oscilloscope for confirmation of laser operation during single shot exposures.

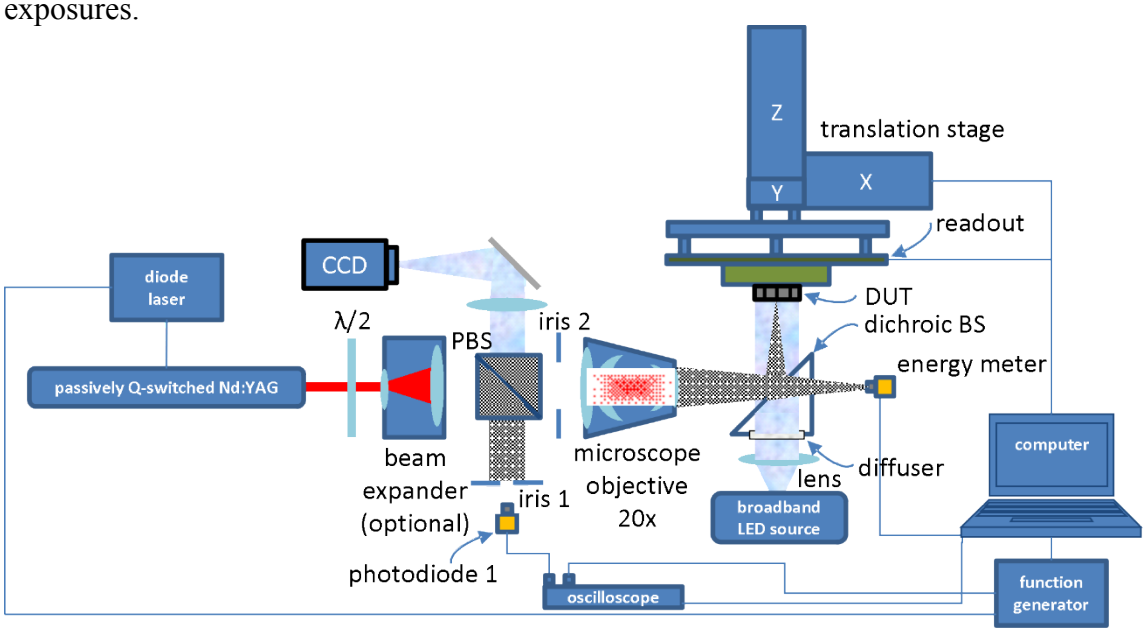

Figure 2. Experimental setup for damaging and laser annealing of Si devices. DUT = device under test, PBS = polarizing beamsplitter.

A 20x NIR microscope objective (NA = 0.28) focuses laser pulses to a spot size of 5 µm (86% encircled energy) at the sample plane. Samples are mounted on a computer controlled XY translation stage with spatial control down to 300 nm. Samples are exposed in the dark to avoid complications of excess carriers due to photo-generation. After a single laser exposure, the photodiode samples undergo a dark IV characterization which is compared to a baseline characterization taken prior to laser exposure. Next the

sample is illuminated with a white light LED and the sample surface is imaged with the CCD. After electrical and surface characterization is complete, the laser fluence is increased and the characterization is repeated.

To find the best laser pulse to anneal with, we first electrically damage our photodiode samples with laser fluence above the damage threshold. We find three separate laser damage thresholds associated with the commercial Si photodiodes used in this study (Hamamatsu S2386-18K). Thresholds are summarized in table 1.

Type of damage	**Multi-shot electrical and morphological damage (20 shots @ 1 Hz)**	**Single shot morphological damage, without electrical damage**	**Single shot electrical and morphological damage**
Threshold	1.1 J/cm^2	1.9 J/cm^2	6.7 J/cm^2

Table 1. Three distinct damage thresholds for Si photodiodes. Multi-shot refers to repeated shots in the same spatial location; morphological and electrical damage occur simultaneously.

Here we define electrical damage as a minimum 10x increase in dark current. Morphological and electrical damage are found to occur simultaneously at a fluence of 1.1 J/cm^2 with multiple shots on the same location, see figure 3. This is in contrast to single shot damage thresholds where surface damage always preceded electrical damage. Morphological damage preceding electrical damage has been observed before [2]; however, for CCDs electrical performance can degrade prior to the onset of surface damage [3].

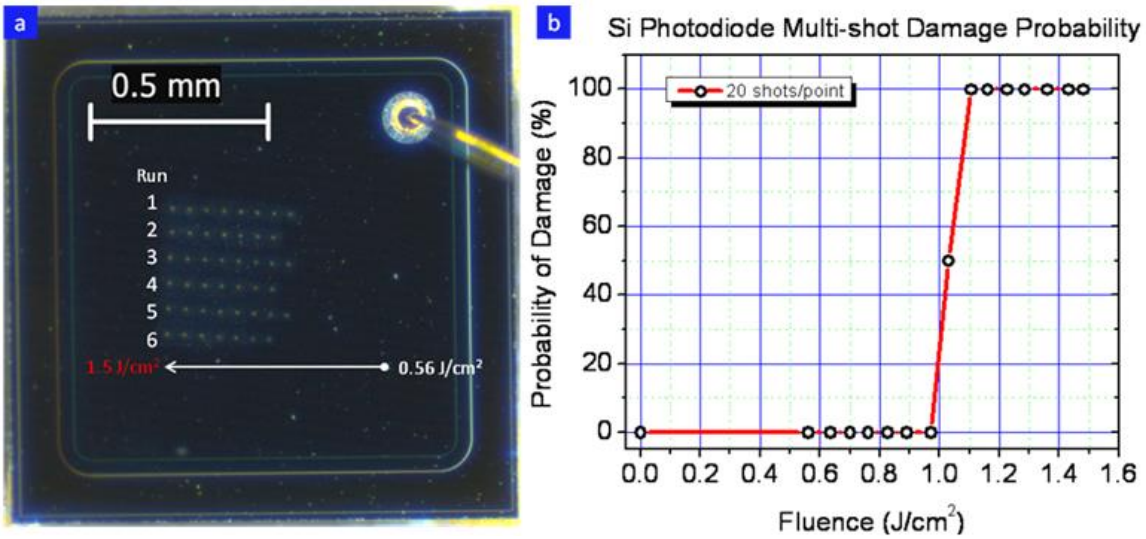

Figure 3. (a) Optical image of photodiode surface after six identical sets of exposures in the fluence range 0.56 to 1.5 J/cm2. Each point was exposed to 20 laser pulses @ 1 Hz. (b) Probability of damage from the fluence data in (a).

For multi-shot investigation the experimental setup is configured to produce one shot every second up to 20 shots. Each shot is at a fixed fluence and at the same location in the active area. With the completion of each 20 shot set, the surface is interrogated for morphological damage and the dark current measured. Electrical and morphological damage were found to occur coincidently in all cases. After a photodiode was damaged it was exchanged with a new one and the measurement repeated. For four different diodes the electrical and morphological damage was found to be coincident. While the damage was coincident for each, the thresholds were slightly different for each, falling in the range 1.05 to 1.58 J/cm2. The slight variation may be due to diode-to-diode variability or small error in placing the surface of the photodiode exactly at the beam waist. Because electrical and morphological damage are coincident with 20 shot exposures, diode-to-diode variability can be circumvented by using a single diode and monitoring it for surface damage at multiple locations. Six successive identical exposures were performed on a single photodiode active area. Starting from a fluence of 0.56 J/cm^2 and progressing across the active area; the fluence is incremented to 1.5 J/cm^2 in 15 even steps. Each fluence increment consists of 20 laser shots at a 1 Hz repetition rate incident on a new spatial location offset by 75 µm. Morphological (and as a corollary, electrical) damage at all higher fluence levels (≥1.1 J/cm^2) is observed in all six exposure sets while no damage was observed for fluence levels at or below 0.98 J/cm^2. The statistical probability of damage from the six runs of fig. 3(a) is plotted in fig. 3(b). Note the sharp transition at 1.1 J/cm^2, which agrees well with other published values for Si [3].

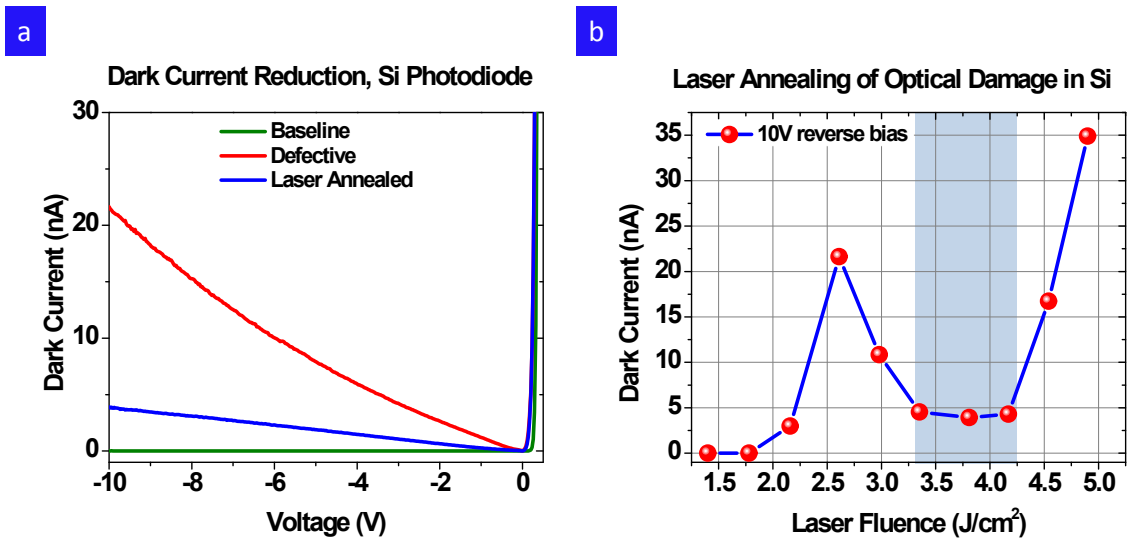

Figure 4. (a) Detector baseline dark current (green line), dark current after damage (red line) and dark current after laser annealing of the damaged site (blue line). Note the substantial reduction (≈5x) in dark current after laser annealing. (b) Dark current after laser exposure, defect creation 2.2 – 2.6 J/cm^2, annealing of created defects 3.25 – 4.25 J/cm^2, irreparable damage >4.25 J/cm^2.

As an example of the power and utility of laser annealing consider the results of figure 4. Our test photodiode is intentionally damaged by a high-energy Q-switched laser pulse onto the active area with a fluence level above the damage threshold. In this instance the damage threshold is different than the values reported in table 1. This is because it is a

ramped fluence multi-shot exposure. That is, each successive laser pulse is of a greater fluence than the preceding pulse. The pulse fluence is continually increased and after each shot the dark current is measured. In this scenario, electrical damage begins at 2.20 J/cm^2, see fig. 4(b). At greater fluence, the dark current continues to increase until 2.6 J/cm^2 after which the dark current begins to decrease. Figure 4(b, shaded region) shows the laser fluence window over which laser annealing takes place and lowers the detector dark current, approximately 3.25 – 4.25 J/cm^2 for a 10 ns, 1064 nm laser pulse. It is, however, important to emphasize that the laser annealing fluence window is device specific; for different detector materials and defects the annealing fluence and laser pulse parameters will change. For fluence in excess of 4.25 J/cm^2 on our device we find the Si boils violently and material ejecta is observed on the photodiode surface. Dark currents only increase after this point and the damage is irreparable. All pulses are incident on the same location. Figure 4(a, red line) shows the increase in dark current above the detector baseline, Fig. 4(a, green line) after the 2.60 J/cm^2 exposure. Photodiode operability is partially recovered with the careful application of an annealing laser pulse directed at the damage area, Fig. 4(a, blue line) after a 3.80 J/cm^2 exposure. More than a 5× reduction in dark current is measured at a reverse bias voltage of -10 volts. Moreover, dark current is reduced for all reverse bias voltages, indicating that detector performance has been improved throughout the IV curve.

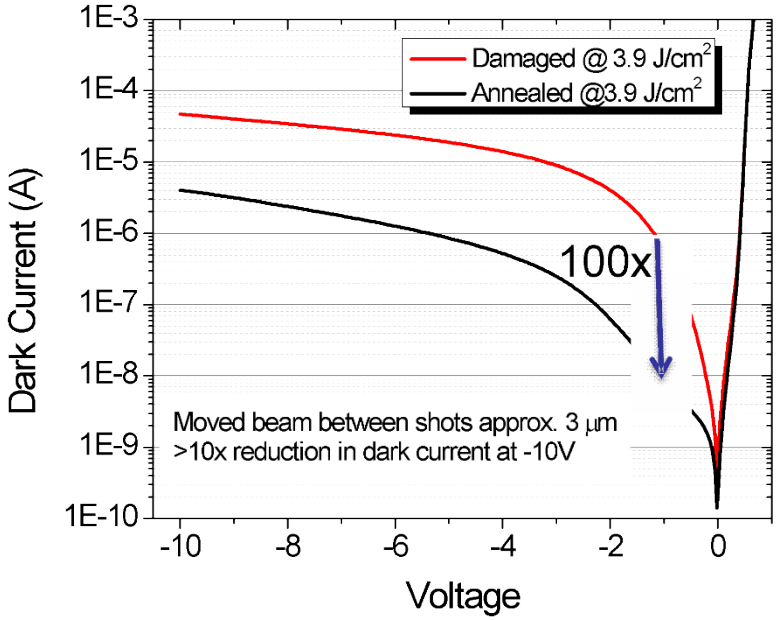

Figure 5. Effect of laser annealing of a damaged detector with a spatial offset between the laser pulse focus and damage site.

With a second series of experiments we consider the effect of spatially offsetting the annealing laser pulse from the damage site. Such an offset allows more undamaged material to be melted and participate in the annealing process. In this case we find an optimum in spatial offset of approximately 3 μm between the damage site and the annealing laser pulse focus. With a spatially offset annealing we were able to achieve a greater than 10x reduction in dark current, see figure 5. Moreover, at low values of

reverse bias (≈1 volt) we were able to demonstrate a 100x decrease in dark current. This is particularly important because many FPAs operate at low reverse bias.

To characterize the damage present in Si after dark current degradation has been measured, we perform cross-sectional SEM analysis of the damage site. Figure 6(left) shows that in the case of an un-annealed damage site, subsurface voids are present near the diode junction (700 nm below the surface). Annealing homogenizes the Si surrounding the junction, removing defects and lowering the dark current, figure 6(right). Images presented in figure 6 are only snapshots of a particular cross-section. We performed focused ion beam (FIB) cutting and SEM analysis across the entire damage site. The un-annealed site had two subsurface voids. The annealed site had none.

Optical damage created here is intentionally created with a laser; but in this instance serves as a means of creating a region of defects and dislocations approximately the same size as a FPA pixel (≈20 μm). Additionally, the laser damage mimics defects and dislocations present in manufactured FPAs from the UV to the IR. Achieving high yield in the manufacturing of some semiconductor detectors is challenging. These results have been demonstrated on Si, but the physics is extensible to other materials where FPAs are often plagued with high dark current and noise.

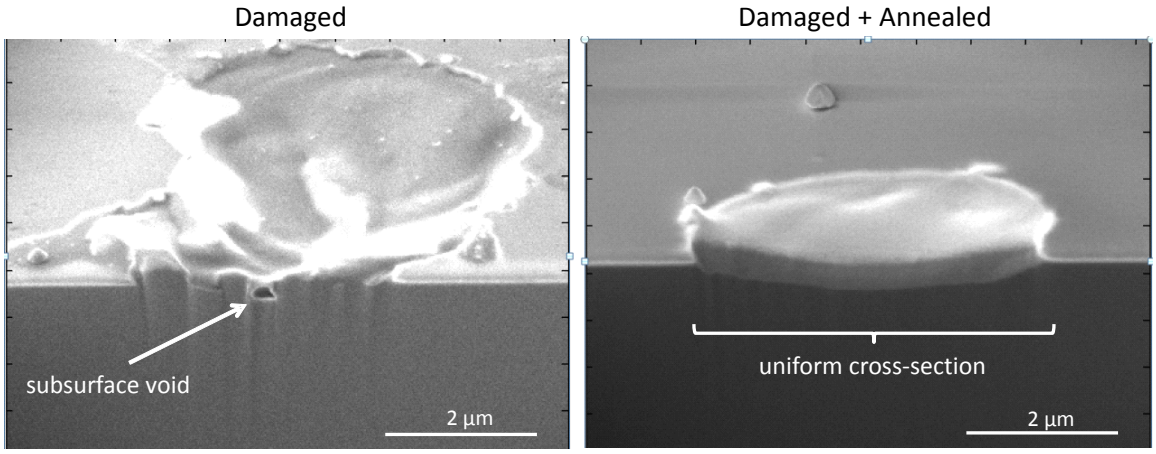

Figure 6. SEM cross-section of damaged and damaged/annealed Si photodiodes. Subsurface voids were found in the case of damage sites that were un-annealed. Homogeneous interfaces were observed between the melt pool and the bulk Si after laser annealing.

Next we consider modification of the optical properties of Si by laser annealing. Specifically, we tune the optical phase acquired in propagation through a single mode waveguide. We fabricate a Mach-Zehnder interferometer out of silicon. One arm of the Mach-Zehnder is shown under magnification in figure 7(a). Broadband coherent light centered at 1550 nm is coupled into the interferometer; output is measured with an optical spectrum analyzer (OSA). The resulting interferogram measured on the OSA is a function of the relative phase difference between each arm of the Mach-Zehnder. A slight change in the optical path length results in a spectral shift of the interference pattern.

Using the same setup detailed in figure 2, we laser anneal small volumes of one arm in the Mach-Zehnder interferometer. To start, a baseline interferogram is measured and recorded with the OSA prior to annealing. Every 10 µm along the propagation axis a single annealing laser pulse is focused onto the waveguide. The pulse fluence varies slightly from shot-to-shot but the mean value is 0.32 J/cm^2 with a standard deviation of 0.0156. After every laser shot the interferogram is re-measured with the OSA and archived. Figure 7(b) shows the evolution of the interferogram for 220 laser shots. After 220 laser shots the phase difference in the interferogram has shifted by a full half wave. This gives an average phase shift of 14.3 mrad per pulse. This level of sensitivity can be used to precisely tune the phase in order to correct for any phase errors that may arise from inhomogeneity in the Si. Furthermore, it is important to note from figure 7(b) that no loss in optical transmission was observed after the 220 laser annealing shots.

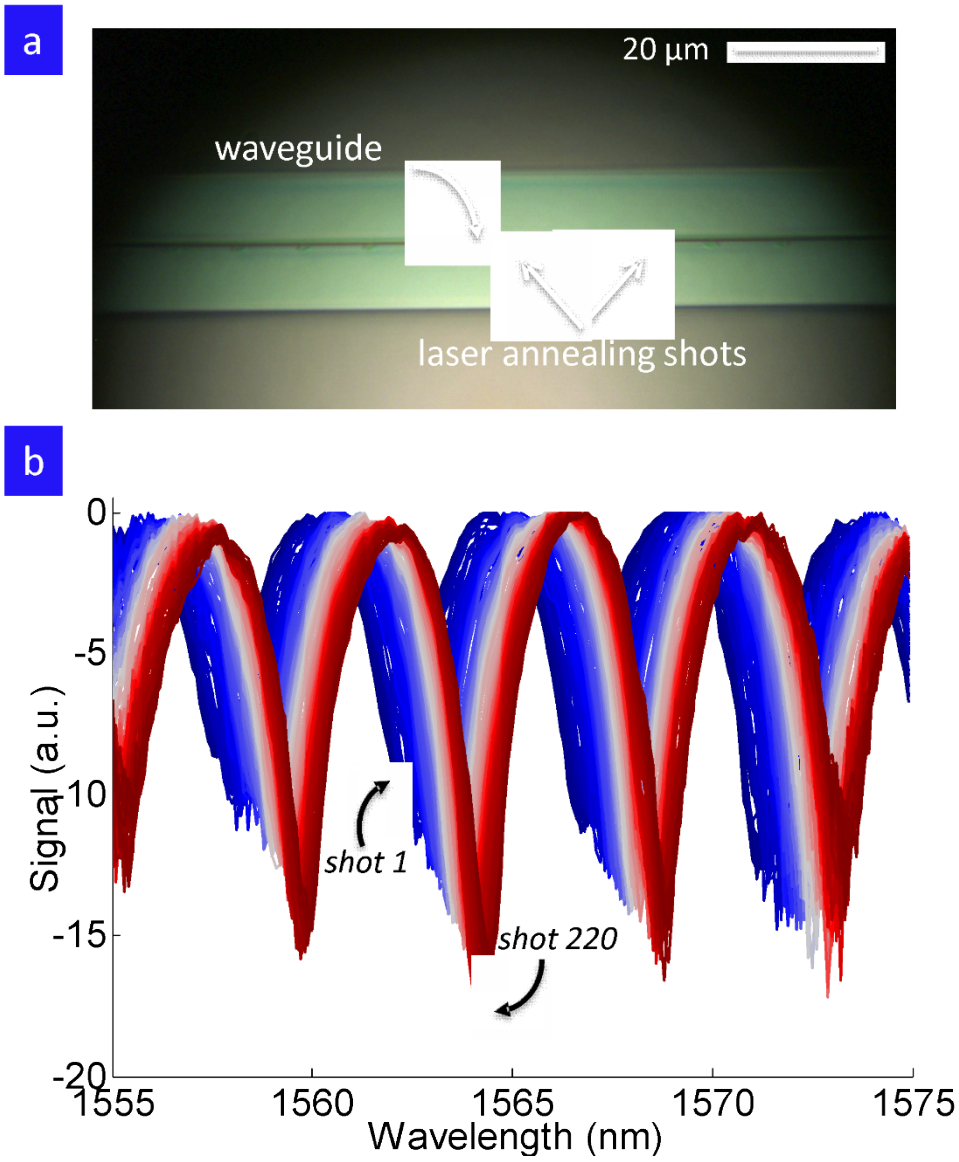

Figure 7. (a) Optical image of a Si waveguide in one arm of a Mach-Zehnder interferometer. Slight melting is seen on the surface of the waveguide, but results in no loss of optical transmission. (b) Series of interferograms measured at the output of the interferometer after each of 220 laser annealing shots; π phase shift is observed.

3. MODEL OF LASER ANNEALING IN SILICON

To inform the experiments, simulations of a laser interaction with a Hamamatsu s2386 photodiode were created using COMSOL Multiphysics. COMSOL is a commercial code for solving generalized partial differential equations using a finite element approach. The simulations were constrained to one-dimension (1D), along the axis of a normal incidence laser beam. The problem required coupling of equations describing the optical, thermal, electrical, and dopant diffusion physics.

The first section in this chapter describes the base equations implemented for each of the physics regimes. The approximations made and their implications are also discussed. The second section gives the results of the simulations.

Simulation Physics

For the simulations, it was assumed that the laser impinged in the central region of the photodiodes, which has a simple structure. As seen in the construction analysis, the central part of the diode consists of a 300 μm thick Si wafer covered by an 80 nm layer of silicon oxide. The silicon has a background phosphorous doping (n-type) of 10^{15} cm^{-3}. A boron (p-type) implant at the surface results in a Gaussian doping profile in the vertical direction, with a maximum doping of 1.7×10^{19} cm^{-3} peaked 175 nm below the surface, and a $1/e$ width of 240 nm.

Optical simulation

The light propagation problem for the ambient and oxide layers was solved analytically. This is because the problem of a single transparent film on a substrate has an analytic solution, and therefore would not require a discretization solution of the electromagnetic partial differential equations (PDEs).

Optically, the silicon diodes have a simple optical structure in the area of interest, with a thick bulk silicon absorption layer covered by a transparent 80 nm silicon oxide film. The amount of light transmitted into the silicon can be calculated from the reflectivity, R as $Tr = 1 - R$. The reflectivity $R = |r|^2$, where the complex reflection coefficient is given by

$$r = \frac{r_{01} + r_{12} e^{i2\beta}}{1 + r_{01} r_{12} e^{i2\beta}}$$

The subscripts {0, 1, 2} correspond to the ambient, film and substrate, where r_{ab} is the reflection coefficient associated with light incident on material *b* from material *a*. β is related to the optical thickness of the oxide film,

$$\beta = 2\pi \frac{d_1}{\lambda} N_1$$

where N_1 is the complex index of refraction, d_1 is the film thickness, and λ is the wavelength of the incident light [4]. After working through the math, the fraction of light transmitted into the silicon is given by

$$\frac{4n_2 N_1^2}{N_1^2(k_2^2 + (n_2+1)^2)\cos^2\beta - 2k_2 N_1(N_1^2 - 1)\cos\beta\sin\beta + (k_2^2 + (n_2 + N_1^2)^2)\sin^2\beta}$$

The optical properties of both the silicon and silicon oxide are dependent on temperature. However, in the simulations only the optical properties of the silicon were made temperature-dependent. In the simulations the reflectivity of the system varies only a few percent for a wide range of temperatures. This is because at 1064 nm the refractive indices change only a few percent, and k_2 is always small relative to N_1 and n_2. However the silicon absorption does change over several orders of magnitude during the simulations, significantly affecting the subsequent heat generation in the silicon.

The absorption coefficient in silicon at 1064 nm is strongly temperature-dependent. This is partially because silicon has an indirect fundamental band gap, which results in a small absorption coefficient at room temperature. As the temperature increases the number of phonons available for phonon-assisted absorption increases dramatically. The equation used for the absorption coefficient in the simulations is [5]

$$\alpha = aT^b, a = 3.13 \times 10^{-10}\ \text{cm}^{-1}\ \text{K}^{-b}, b = 4.25,$$

In addition to absorption due to electronic transitions, free carrier absorption can become significant at large carrier densities (which can be due to high doping levels or high optical intensities). The temperature dependence of the free-carrier absorption cross-section is given by [2]

$$\sigma = sT, s = 1.7 \times 10^{-20}\ \text{cm}^2\ \text{K}^{-1}$$

The resulting imaginary part of the index of refraction for silicon, k_2, is given by

$$k_2 = \frac{\lambda}{4\pi}(\alpha + \sigma U)$$

where *U* is the net carrier density due to optical generation and doping. Other treatments of laser heating [6] have explicitly included two-photon and intervalence band absorption in addition to one-photon and free-carrier absorption described above. However, the

above treatment is taken from Nilsson and Svantesson[5], who derived their expressions from measurements. Therefore, the second-order effects could be considered as implicitly included in the given expressions.

Following Jellison and Modine [7], the real part of the index of refraction for a wavelength of 1064 nm is given by

$$n = [12.2 + 0.00176\,T]^{1/2}$$

The Jellison and Modine paper describes data for wavelengths up to 844 nm, so the above expression for 1064 nm is an extrapolation; but the extrapolation is not an unreasonable one since the index of refraction of silicon is monotonic and changes slowly in that range of wavelengths.

The heat generation is directly related to the attenuation of the intensity in the substrate. This is coupled to the carrier density and temperature as

$$\frac{\partial I}{\partial z} = -(\alpha + \sigma U) I$$

where $I(z)$ is the light intensity as a function of depth in the silicon. This is one of the four coupled PDEs solved by COMSOL. Any light that makes it to the backside of the silicon is assumed to be lost (i.e., backside reflections are not taken into account). Since the majority of the light is absorbed in the top 100 nm of the device (as seen in the simulation results), this approximation is reasonable. The boundary condition at the surface is $I(0) = (1 - R)I_0$, where I_0 is the incident light intensity.

Thermal physics

The thermal model is based on the standard heat equation, which is one of the PDEs solved by COMSOL:

$$\frac{\partial T}{\partial t} = \frac{\kappa}{\rho c_p}\nabla^2 T + \frac{G}{\rho c_p}$$

where ρ is the density, c_p is the specific heat and κ is the thermal conductivity. The heat generation rate per unit volume, *G*, is given by [5]

$$G = \sigma U I + \frac{u}{\tau}E_g + \left(E_{ph} - E_g\right)\frac{\alpha I}{E_{ph}}$$

The first term is due to the free-carrier absorption, the second is from electron-hole recombination, and the third is from the energy due to the relaxation of the carriers to the top/bottom of the valence/conduction bands. The excess carrier density due to photogeneration is *u*, τ is the carrier lifetime, E_g is the band gap energy of the silicon and E_{ph} is the energy of the incoming photons. The top of the oxide is assumed to be

insulating (i.e., no heat is transferred to the air), and the backside of the silicon is assumed to be at room temperature.

The relaxation term includes the assumption that carrier relaxation is much faster than the carrier movement through the silicon. This allows the instantaneous creation of heat via relaxation of the carriers to the band edge. Since the relaxation time is on the order of femtoseconds, the approximation is not unreasonable.

Boron diffusion

The diffusion of the boron follows the standard diffusion equation, with no generation or loss

$$\frac{\partial N}{\partial t} = D_B \nabla^2 N$$

The diffusion coefficient is temperature-dependent as in

$$D_B = D_0 e^{-E_{act}/k_B T}$$

where E_{act} is the diffusion activation energy and k_B is Boltzmann's constant. This is the third PDE simulated in COMSOL.

Excess carrier density

The density of the excess carriers in the silicon can be calculated using several different approaches that have varying levels of approximation. Simulation efforts that predated this one used the drift-diffusion formulation prevalent in TCAD codes [8]. TCAD is the typical simulation approach for individual semiconductor devices, such as MOSFETs and BJTs; but it is computationally expensive and not stable in the standard finite element formalism for solving PDEs. One of the outcomes of those simulations, though, indicated that at high optical intensities, the carrier generation density is high enough to overwhelm and eliminate the built-in electric field present at all p-n junctions. This creates an opportunity to take a simpler simulation approach by using the ambipolar diffusion equation (ADE), which is the fourth PDE solved in COMSOL.

The ADE is derived from the drift-diffusion equations by making the assumption that the distributions of the excess electrons and holes are approximately equal. In cases of large carrier generation rates, this is an excellent approximation. Taking the assumption of no electric field, the ADE can be written as

$$\frac{\partial u}{\partial t} = D_a \nabla^2 u - \frac{u}{\tau} + g$$

where the carrier generation rate, *g*, is given by

$$g = \frac{\alpha I}{E_{ph}}$$

D_a is the ambipolar diffusivity, and τ is the effective carrier lifetime. While both D_a and τ could depend on the carrier densities, they are approximately constant for large excess carrier densities.

Simulation Results

The following simulation results are for a laser having a Gaussian temporal profile with a peak intensity of 1.5×10^8 W cm^{-2} and a $1/e$ width of 10 ns. While the choices of material parameters (such as boron diffusivity or carrier lifetimes) affect the results, the overall trends are accurate.

Figure 8 and Figure 9 show temperature as a function of time for various locations in the device. The silicon-silicon oxide interface is defined as $z = 0$, with z increasing as a function of depth in the device. The temperature increases rapidly near the surface, but the initial temperature increase is small below 25 µm (Figure 8). As the heat and generated carriers diffuse through the bulk, though, there is a noticeable temperature increase up to 100 µm below the surface. If the heat transfer into the air were taken into account, the temperature increase would likely be more confined to the surface regions.

As would be expected from the temperature graphs, the heat generation is strongly confined to the top 20 µm of the device. This can be seen in Figure 10. Notice that almost all of the heat generation occurs in a 20 ns window, which is on the order of the laser pulse width.

Figure 11 shows the optical intensity in the silicon as a function of time for several depths in the silicon. The intensity at the surface (0 nm) is closely representative of the actual laser pulse, but is modified by the slight changes in reflectance. Note that the intensity starts to build throughout the device, but as the carrier density and temperature increase, the intensity becomes confined to the top layers of the device. Figure 12 shows the combined absorption coefficient $(\alpha + \sigma U)$ as a function of time. Due to the short pulse time, much of the increase in the combined absorption coefficient occurs after the pulse is over. It is also worth noting that the heat generation lags the optical excitation by about 8 ns.

Figure 13 shows the excess carrier density as a function of time. The overall curve shapes are similar to the temperature curves, but that is likely due to the fact that similar equations (diffusion/heat) govern both phenomena. Almost all the carrier generation is in the top 10–20 µm of the device; the curves greater than 20 µm increase well after the pulse has ended, indicating the carrier increase in that region is due to diffusive rather than generation effects. The use of the full drift-diffusion equations would likely show different longer-term behavior because the built-in electric field at the p-n junction would eventually re-form and sweep some carriers out of the device and to the contacts.

The distribution of the boron dopant in the device at various times is shown in Figure 14. The concentration changes very little during the pulse, which is not surprising since the maximum temperature in the device is much lower than typical semiconductor processing

dopant annealing steps (which are on the order of 1000–1200 K). However, there is a small amount of spreading during the simulation, mostly toward the surface.

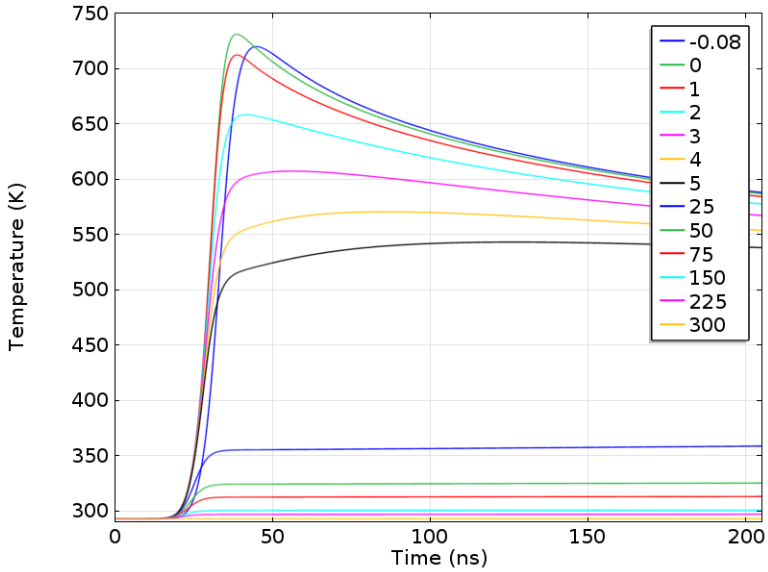

Figure 8: Temperature as a function of time at several locations in the device in the first

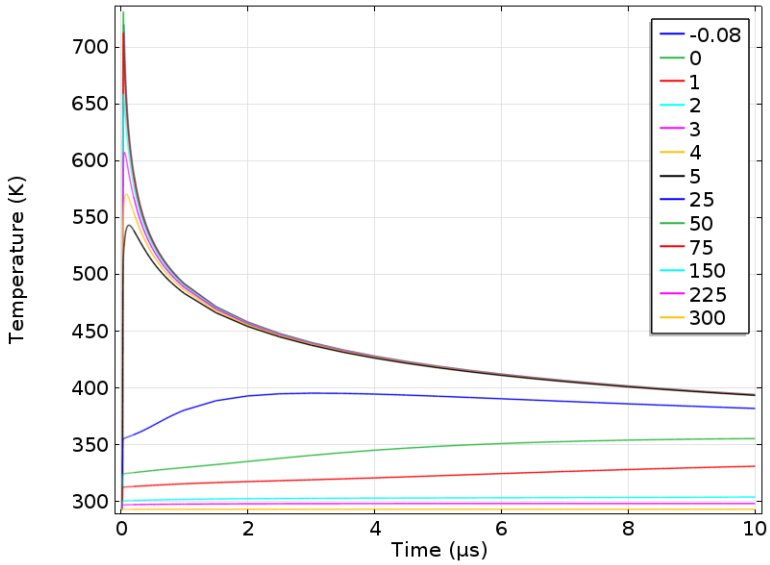

Figure 9: Temperature as a function of time at several locations in the device

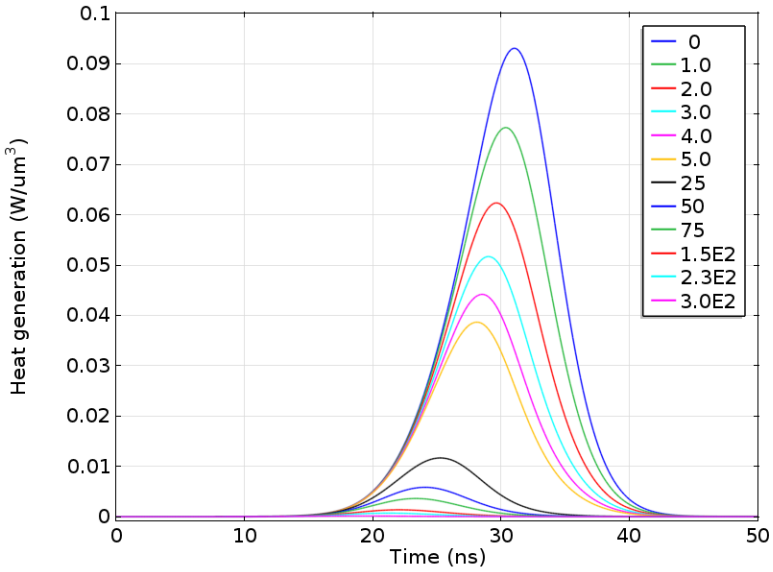

Figure 10: Heat generation as a function of time at several locations in the device

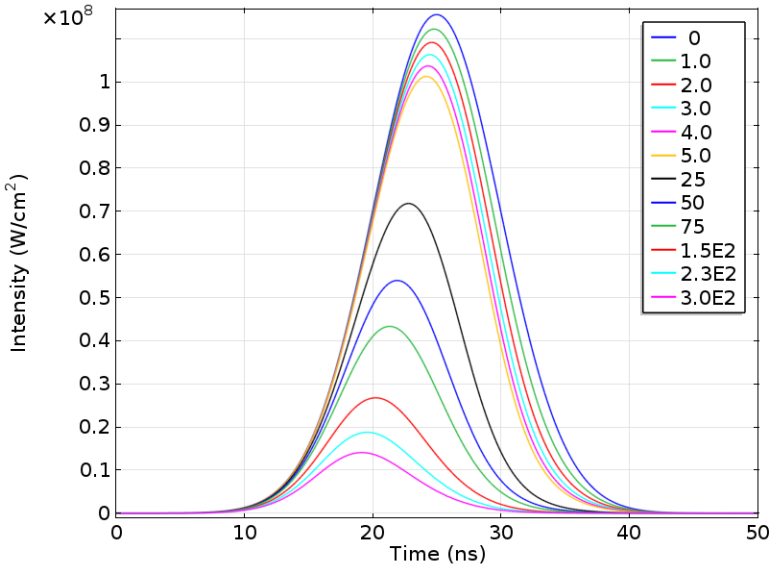

Figure 11: Optical intensity as a function of time at several locations in the device

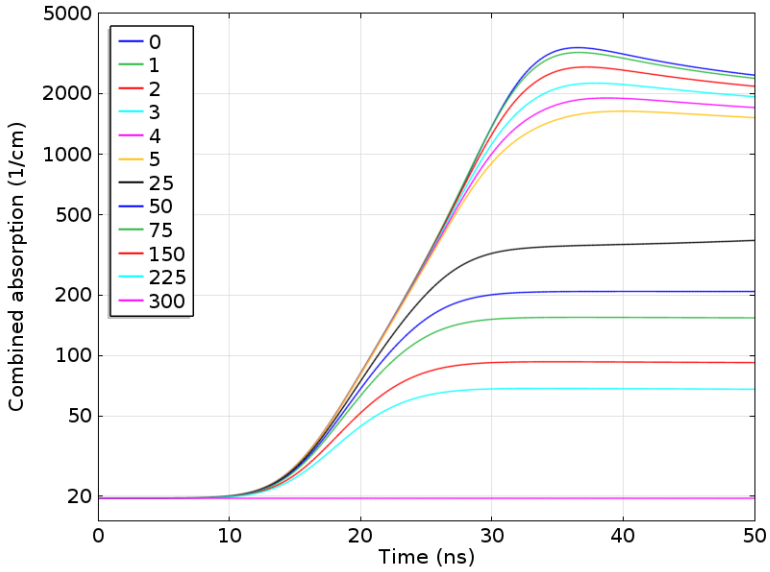

Figure 12: Combined absorption coefficient $(\alpha + \sigma U)$ as a function of time at several locations in the device

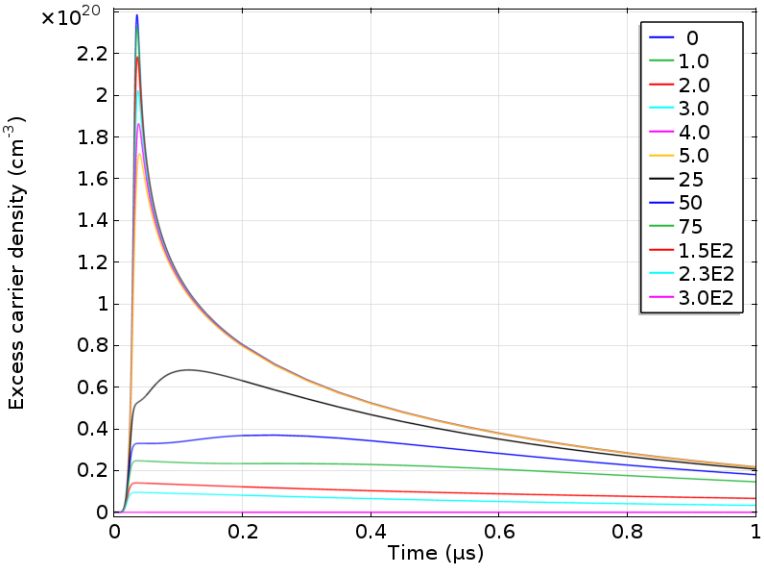

Figure 13: Excess carrier density as a function of time at several locations in the device

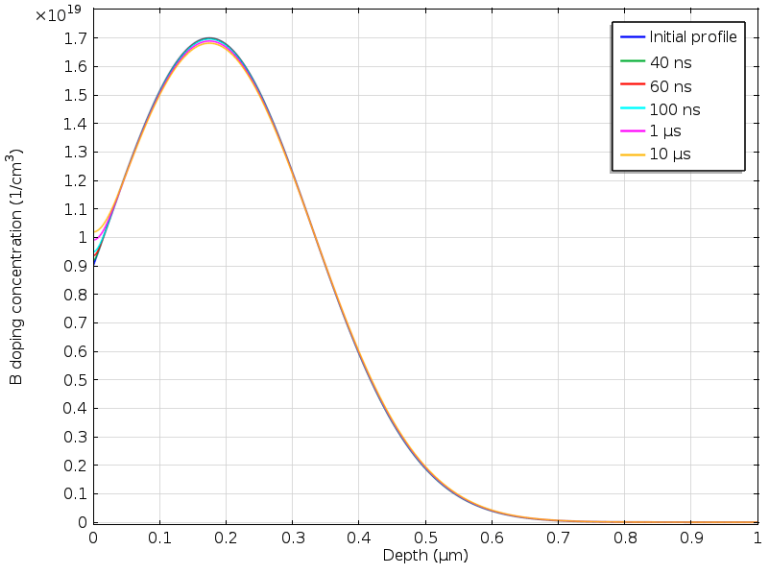

Figure 14: Boron concentration as a function of depth at various times

Discussion

In silicon with a 1064 nm laser, a longer pulse would be more effective at confining the heating to the top layer. Other changes that would increase the heating in the silicon would be to use a shorter wavelength laser (absorption increases markedly in the near UV due to the onset of direct band transitions), or a longer pulse with the intensity tuned to not melt the material. Any of this would enhance the boron diffusion.

Direct band gap materials—such as most III-V and II-VI compound semiconductors—have a much higher optical absorption as long as the photon energy is higher than the band gap. Absorption in these materials naturally occurs near the surface.

4. SUMMARY

We have presented results from laser annealing experiments in Si using a passively Q-switched Nd:YAG microlaser. Operating the laser at fluence values above the damage threshold of commercially available photodiodes results in electrical damage (as measured by an increase in photodiode dark current). We show that increasing the laser fluence to values in excess of the damage threshold can result in annealing of a damage site and a reduction in detector dark current by as much as 100x in some cases. A still further increase in fluence results in irreparable damage. Thus we demonstrate the presence of a laser annealing window over which performance of damaged detectors can be at least partially reconstituted. Moreover dark current reduction is observed over the entire operating range of the diode indicating that device performance has been improved for all values of reverse bias voltage. Additionally, we have presented results of laser annealing in Si waveguides. By exposing a small (<10 um) length of a Si waveguide to an annealing laser pulse, the longitudinal phase of light acquired in propagating through the waveguide can be modified with high precision, <150 milliradian per laser pulse. Phase tuning by 180 degrees was exhibited with multiple exposures to one arm of a Mach-Zehnder interferometer at fluence values below the morphological damage

threshold of an etched Si waveguide. No reduction in optical transmission at 1550 nm was found after 220 annealing laser shots.

Finally, we presented a multiphysics model taking into account temperature dependent electro-optic properties of Si for modeling of junction temperature during and boron diffusion laser annealing.

5. REFERENCES

[1] J. Yan, *et. al*., "Response of machining-damaged single-crystalline silicon wafers to nanosecond pulsed laser irradiation," *Semi. Sci. & Tech*., **22**, pp. 392-395, (2007).

[2] S. E. Watkins, *et. al*., "Electrical performance of laser damaged silicon photodiodes," *Applied Optics*, **29**, pp. 827-835, (1990).

[3] C. Zhang*, et. al.,*"Laser-induced damage to silicon charge-coupled imaging devices," *Optical Engineering*, **30**, No. 5, pp. 651-657, (1991).

[4] R. M. A. Azzam and N. M. Bashara, "Ellipsometry and Polarized Light," Elsevier (Amsterdam, 1977).

[5] N. G. Nilsson and K. G. Svantesson, "The role of free carrier absorption in laser annealing of silicon at 1.06 μm," J. Phys. D : Appl. Phys., 13 (1980) 39-44.

[6] A. K. Storeboe, T. Brudevoll and K. Stenersen, "Calculated temperature rise in midinfrared laser irradiated Hg0.72Cd0.28Te," J. Appl. Phys. 103, 053108 (2008).

[7] Jellison and Modine, "Optical functions of silicon at elevated temperatures," J. Appl. Phys. 76, 3758 (1994).

[8] T. Beechem, et al., "Laser Characterization and Prediction for Silicon Sensors," Report SAND2012-7777, Sandia National Labs (2012).

DISTRIBUTION:

1	MS0359	Donna Chavez, 7911
1	MS0980	Daniel A. Bender, 5774
1	MS1081	Mark Jenkins, 1755
1	MS1082	Christopher DeRose, 1765
1	MS1084	Andrew Starbuck, 1768
1	MS1177	Jason Verley, 1355
1	MS0899	Technical Library, 9536 (electronic copy)


Sandia National Laboratories